

IAC-12-C1.9.6

## DUAL ATTITUDE AND PARAMETER ESTIMATION OF PASSIVELY MAGNETICALLY STABILIZED SPACECRAFT

**R. Burton**

Stanford University, USA, [rolandb@stanford.edu](mailto:rolandb@stanford.edu)

S. Rock\*, J. Springmann†, J. Cutler‡

Precision attitude determination of a nano satellite is limited by a lack of traditional high performance attitude sensors, a result of having small budgets for mass and power. Attitude determination can still be performed on a nano satellite with low fidelity sensors, but an accurate model of the dominant torques acting on the spacecraft is required to achieve precision. Many nano satellites use passive magnetic stabilization systems consisting of a combination of a permanent dipole for alignment to the local magnetic field and magnetically permeable material for damping. The torques generated by a passive magnetic system are dependent on the effective magnetic properties of the installed components, and these cannot easily be measured prior to launch. Spacecraft attitude cannot be determined accurately until these effective properties are calibrated on orbit. In this paper, an estimation problem is formulated that simultaneously solves for the attitude of the spacecraft and performs parameter estimation on the magnetic properties of the magnetic materials. The estimation technique is applied to data from NASA Ames Research Center's O/OREOS nano satellite and the University of Michigan's RAX-1 nano satellite, where clear differences are detected between the magnetic properties as measured before launch and those that fit the observed data. To date this is the first known on-orbit verification of a dynamics model for passively magnetically stabilized spacecraft.

### I. INTRODUCTION

On large spacecraft, high precision attitude determination can be performed using high performance sensors such as star trackers and inertial grade gyros. On small spacecraft, however, such instrumentation is typically not available due to small budgets for power, mass and volume. Precision attitude determination can still be per-

formed on a nano satellite with fewer, lower performance sensors, but an estimator that incorporates an accurate spacecraft attitude dynamics model is required.

The same low mass and power budgets that negate the use of high performance attitude sensors also encourage the use of passive magnetic stabilization systems in nano satellites. These passive magnetic systems require no power and have low mass and volume requirements. Passive magnetic systems typically consist of a permanent dipole that provides alignment to the Earth's magnetic field, and magnetically permeable material that provides damping for the removal of excess rotational kinetic energy. An accurate attitude dynamics model for a passively magnetically stabilized spacecraft requires an accurate model of the torques generated from the interaction of these magnetic components with the Earth's magnetic field.

While the torque arising from a permanent dipole of known strength in an external magnetic field is trivially computed, the magnetically permeable material poses more of a challenge due to non-linear time-variant dynamics and the presence of additional states that are not directly observable. These dynamics have been studied well for isolated samples of material in a laboratory,<sup>1</sup> and in such situations the material's properties can be accurately characterized. To date there has been no demonstration of the fidelity of these models when included in a full attitude dynamics simulation.

When the magnetic components are installed in a

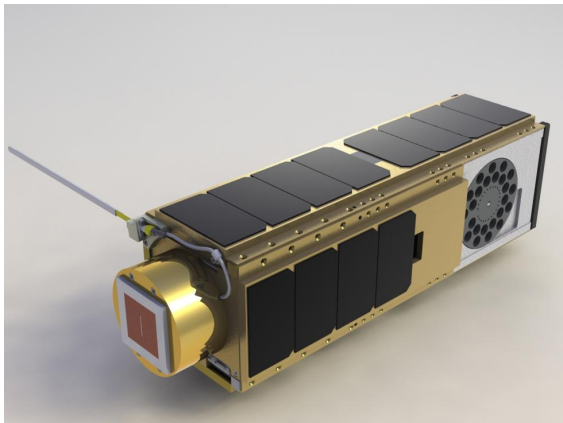


Figure 1: NASA Ames Research Center's O/OREOS 3U CubeSat. An example of a passively magnetically stabilized spacecraft

\*Stanford University, USA, [rock@stanford.edu](mailto:rock@stanford.edu)

†University of Michigan, USA, [jspringm@umich.edu](mailto:jspringm@umich.edu),  
[jwcutler@umich.edu](mailto:jwcutler@umich.edu)

spacecraft the magnetic properties will change due to interactions both with similar material installed in close proximity, and also to other spacecraft components. Pre-launch testing in the laboratory of a complete system is hampered by the very small torques produced, and the difficulty in maintaining a magnetically clean environment. The differences between laboratory measured properties and the effective installed properties have been substantial enough to cause problems with attitude determination, with previous nano satellite missions observing disagreements between pre-launch simulations and observed attitude profiles.<sup>2</sup>

An alternative approach to characterizing the magnetic properties and to obtain an accurate attitude dynamics model is to calibrate the magnetic properties using on-orbit data. Specifically parameter estimation can be performed to fit a dynamics model to observed data. As the on-orbit measurements will be attitude dependent, the attitude determination and parameter estimation problems need to be solved simultaneously.

## II. METHOD

The estimation problem can be described as finding a set of initial conditions and parameters that reproduces the measured data as closely as possible. This can be formulated as an optimization problem for a dynamical system (Equation [1]), where initial conditions and system parameters are iterated upon until simulated data matches measured data.

$$\begin{aligned} & \underset{x_0, \theta}{\text{minimize}} && \sum J(x(t), t) && t = 0, \dots, T. \\ & \text{subject to} && \dot{x}(t) = f(x(t), \theta, t) \\ & && x(0) = x_0 \\ & && c_i(x_0, \theta) \leq 0, && i = 1, \dots, m. \\ & && c_{eq_j}(x_0, \theta) = 0, && j = 1, \dots, n. \end{aligned} \quad [1]$$

The function  $f(x(t), \theta, t)$  describes the attitude dynamics of a passively magnetically stabilized spacecraft. The state  $x(t)$  includes both the kinematic state and an additional state required to model the time variant behavior of the magnetic material. The parameters of the dynamical system  $\theta$  are any constants in the state dynamics that are unknown or require calibration, and in this work are the properties of the magnetic materials in the system.

The constraints  $c_i(x_0, \theta)$  and  $c_{eq_j}(x_0, \theta)$  ensure that the parameters  $\theta$  and the initial state  $x_0$  are physically realizable.

The cost function  $J(x(t), t)$  is the difference between actual measurements recorded by the spacecraft, and the value of those measurements as generated by propagating the dynamics in simulation.

## II.I Attitude Dynamics

$$\dot{q} = \frac{1}{2} \omega \otimes q \quad [2]$$

$$T = I\dot{\omega} + \omega \times I\omega \quad [3]$$

The attitude kinematics and dynamics are given by Equations [2] and [3]. The unit quaternion is used to represent the spacecraft's attitude and  $\omega$  is the body angular rate in the body frame. As moments of inertia can be accurately measured prior to launch, in this work it is assumed that the inertia  $I$  of the spacecraft is known and is not included as an optimization parameter.

In Equation [3] the external torque  $T$  includes parasitic environmental torques in addition to any control torques. In the case of a passively magnetically stabilized spacecraft these control torques will arise from the interaction of the dipoles with the Earth's magnetic field. Typical expected values of the environmental torques were estimated for a 3U ( $30 \times 10 \times 10 \text{cm}^3$ ) cubesat in a 650km low Earth orbit and are listed in Table 1, along with nominal values for the torques from a typical passive magnetic stabilization system. As the parasitic torques are several

Torque Source	Nominal Value ( $\text{Nm}^{-1}$ )
Permanent Dipole	$7 \times 10^{-4}$
Saturated Permeable Rod	$1 \times 10^{-5}$
Gravity Gradient	$7 \times 10^{-8}$
Solar Radiation Pressure	$2 \times 10^{-8}$
Aerodynamic Pressure	$2 \times 10^{-9}$

Table 1: Torques acting on the spacecraft

orders of magnitude lower than those from the magnetics, it is reasonable to ignore them in the dynamics model.

The torque from a dipole of strength  $M$  in a magnetic field  $H$  is given by Equation [4] where  $\mu_0$  is the permeability of free space. In a system comprising of both permanent dipoles and magnetically permeable material the torque can be computed using Equation [5] where  $M_P$  is the strength of the permanent dipole, and  $B$  is the induced flux density in a permeable rod of volume  $V$ .

$$T = \mu_0 (M \times H) \quad [4]$$

$$= (BV + \mu_0 M_P) \times H \quad [5]$$

The external magnetic field  $H$  is assumed to be known, and can be computed if the spacecraft's orbital position is known. The effective installed permanent dipole  $M_P$  and the effective permeable rod volume  $V$  are both assumed to be unknown constant parameters. The induced magnetic flux density in the rod  $B$  is time variant, so the state dynamics  $f(x(t), \theta, t)$  must include the dynamics of the permeable material to allow the torque to be computed.

## II.II Hysteresis Modeling

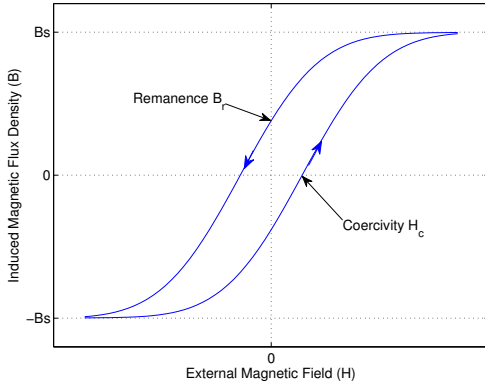


Figure 2: Typical Hysteresis Loop

If a permeable rod is placed in a time varying magnetic field with component  $H$  along the long axis of the rod, the flux density induced in the rod  $B$  lags changes in the external field, a phenomenon known as hysteresis. The three magnetic properties of permeable material that describe the shape of these hysteresis loops, as illustrated in Figure 2, are: the saturation flux density  $B_s$ ; the remanence flux density  $B_r$ ; and the coercivity  $H_c$ .

Flatley and Henretty<sup>1</sup> proposed an empirical model to describe both the bounding curves of the hysteresis material and the behavior between the two curves. The bounding curves are described by the inverse tangent function Equation [6]. Equation [7] is the empirically derived differential equation that describes the behavior at any point  $(H, B)$  between the limits. The derived material property  $k$  is called the shape parameter. A sample simulated hysteresis loop is illustrated in Figure 3 where the external field was varied between  $\pm H_c$ .

$$B_{lim}(H) = B_s \left( \frac{2}{\pi} \right) \arctan(k(H \pm H_c)) \quad [6]$$

$$\frac{dB}{dH} = \frac{2}{\pi} k B_s \cos^2 \left( \frac{\pi B}{2 B_s} \right) \left( \frac{H - H_{lim}(B)}{2 H_c} \right)^2 \quad [7]$$

where

$$k = \frac{1}{H_c} \tan \left( \frac{\pi B_r}{2 B_s} \right) \quad [8]$$

$$H_{lim}(B) = \frac{1}{k} \tan \left( \frac{\pi B}{2 B_s} \right) \pm H_c \quad [9]$$

If both the component of the external field aligned with the rod  $H$ , and the time rate of change of this component  $\dot{H}$  are known then magnetically permeable material can be included in a dynamical system by augmenting the existing states with the induced flux density  $B$  and augmenting

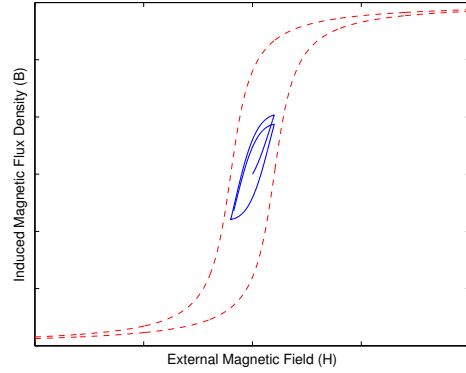


Figure 3: Simulation of Hysteresis Loop

the state update equations with Equation [10].

$$\frac{dB}{dt} = \frac{dB}{dH} \frac{dH}{dt} \quad [10]$$

In the case of the attitude dynamics simulation, the kinematic state  $(q, \omega)$  is augmented with three  $(x, y, z)$  components of induced magnetic flux to account for rods aligned with the three body axes.

It has been shown<sup>3</sup> that significant computational advantages are obtained by integrating a substituted modified flux state  $S$  as defined in Equation [11] rather than directly integrating  $B$ .

$$S = \tan \left( \frac{\pi B}{2 B_s} \right) \quad [11]$$

The bounding limits and differential equation describing the behavior between the limits are described in Equations [12] and [13] respectively. Integrating  $S$  rather than  $B$  involves fewer transcendental function evaluations and operations close to  $(\tan \frac{\pi}{2})$ .

$$S_{lim} = k(H \pm H_c) \quad [12]$$

$$\frac{dS}{dH} = k \left( \frac{H - \frac{S}{k} \pm H_c}{2 H_c} \right)^2 \quad [13]$$

$$\frac{dS}{dt} = \frac{dS}{dH} \frac{dH}{dt} \quad [14]$$

The substitution offers faster numerical convergence, allowing a larger integration time step and an order of magnitude improvement in integration speed. This speed increase becomes of great value in iterative optimizations or sequential Monte-Carlo methods.

## II.III External Magnetic Field

Computation of the torque also requires knowledge of the external magnetic field in the body frame. The computation of the dynamics of the induced magnetic flux den-

sity in the rod (Equation [10] or [14]), additionally requires knowledge of the time rate of change of the external field.

Assuming the spacecraft's orbital position is known, then the external magnetic field in an inertial frame  $H_{ECI}$  can be computed from the IGRF<sup>4</sup> model. If it is assumed that the orbital position is independent of the spacecraft's attitude then the spacecraft's orbital position can be propagated independently and a time derivative of the magnetic field  $\dot{H}_{ECI}$  computed. From these the external magnetic field  $H$  and its time derivative  $\dot{H}$  in the body frame can then be calculated using Equations [15] and [16] respectively.

$$H = q \otimes H_{ECI} \otimes q^{-1} \quad [15]$$

$$\dot{H} = q \otimes \dot{H}_{ECI} \otimes q^{-1} - \omega \times H \quad [16]$$

Spacecraft position is typically obtained from two-line element (TLE) ephemerides. Propagation can then be performed from TLEs using the SGP4<sup>5</sup> algorithm.

#### II.IV Summary of Attitude Dynamics

The full attitude dynamics of a passively magnetically stabilized spacecraft are summarized in Equation [17].

$$\begin{aligned} \dot{q} &= \frac{1}{2} \omega \otimes q \\ \dot{\omega} &= I^{-1} \left( \left( \frac{2}{\pi} B_s V \arctan(S) + \mu_0 M_P \times H \right) - \dots \right. \\ &\quad \left. \omega \times I \omega \right) \\ \dot{S} &= k \dot{H} \left( \frac{H - \frac{S}{k} \pm H_c}{2H_c} \right)^2 \end{aligned} \quad [17]$$

where

$$H = q \otimes H_{ECI} \otimes q^{-1}$$

$$\dot{H} = q \otimes \dot{H}_{ECI} \otimes q^{-1} - \omega \times H$$

The state  $x$  and time derivative of the state  $f(x(t), \theta, t)$  as required in Equation [1] are defined in Equations [18] and [19], and the parameters  $\theta$  are defined by Equation [20].

$$x(t) = \begin{bmatrix} q(t) \\ \omega(t) \\ S(t) \end{bmatrix} \quad [18]$$

$$f(x(t), \theta, t) = \dot{x}(t) = \begin{bmatrix} \dot{q}(t) \\ \dot{\omega}(t) \\ \dot{S}(t) \end{bmatrix} \quad [19]$$

$$\theta = \begin{bmatrix} M_P \\ B_s \\ B_r \\ H_c \\ V \end{bmatrix} \quad [20]$$

#### II.V Cost Function

As this work is intended to be applied to low cost nano satellites, it is assumed that the only measurement available is the sun vector. Even when the spacecraft has no dedicated sun sensors, an estimate of the solar vector can be made from the body mounted solar panel currents. The scalar cost function at each time step  $J(x(t), t)$  is defined by Equation [21] and is the norm of the difference between the sun vector measured by the bus  $c_{bus}$  and the sun vector in the inertial frame  $c_{ECI}$  rotated to the body frame.

$$J(x(t), t) = \|q(t) \otimes c_{ECI}(t) \otimes q(t)^{-1} - c_{bus}(t)\| \quad [21]$$

#### II.VI Constraints

The parameters and initial conditions must be constrained to physically realizable values. If the dynamics of the system are correctly formulated, the system is stable and  $x_0$  is physical, then the state  $x(t)$  will stay physically realizable and does not need to be explicitly constrained. For the passively magnetically stabilized spacecraft these physical limits are summarized in Equation [22].

$$\begin{aligned} -B_s &\leq 0 \\ -B_r &\leq 0 \\ -H_c &\leq 0 \\ B_r - B_s &\leq 0 \\ S(0) - k(H(0) - H_c) &\leq 0 \\ -k(H(0) + H_c) - S(0) &\leq 0 \\ \|q(0)\| - 1 &= 0 \end{aligned} \quad [22]$$

#### II.VII Simplifications

The optimization problem as described so far in Section II can be further simplified by realizing that some variable substitution can reduce both the dimension size and the number and complexity of the constraints. If the initial attitude  $q(0)$  is replaced with a three-component attitude parameterization such as Euler Angles, this reduces the state size by one and removes the non-convex equality constraint that requires  $q(0)$  to be of unit length.

The remaining non-convex constraints involving  $S(0)$ ,  $k$  and  $H_c$  can be removed by introducing a new variable  $s_0$  as defined in Equation [23]. The new variable  $s_0$  denotes the fractional position that  $S(0)$  lies between the limiting substituted flux densities  $S_{lim}$  evaluated at  $H(0)$ , with values of  $\pm 1$  denoting the limits. The modified flux parameter initial condition  $S(0)$  can be recovered using Equation [24].

$$s_0 = \frac{S(0) - kH(0)}{kH_c} \quad [23]$$

$$S(0) = k(s_0 H_c + H(0)) \quad [24]$$

Examination of Equation [17] reveals that the parameters  $B_s$  and  $V$  only ever appear together as the product

$B_s V$ . As such they are independently unobservable and can be replaced by a new parameter  $B_s V$ . The constraint that  $B_r < B_s$  now cannot be explicitly enforced so a new non-dimensional parameter  $\nu$  is introduced as defined in Equation [25], taking advantage that  $B_r$  is only used in defining the shape parameter  $k$ . The only constraint on  $\nu$  is that it be positive.

$$\nu = \tan\left(\frac{\pi B_r}{2 B_s}\right) = k H_c \quad [25]$$

## II.VIII Optimization Problem

The resulting optimization problem specific to a passively magnetically stabilized spacecraft is summarized in Equations [26] and [27].

$$\begin{aligned} & \underset{\tilde{x}_0, \theta}{\text{minimize}} && \sum J(x(t), t) \\ & \text{subject to} && \dot{x}(t) = f(x(t), \theta, t) \\ & && x(0) = g(\tilde{x}_0) \\ & && -B_s V \leq 0 \\ & && -H_c \leq 0 \\ & && -\nu \leq 0 \end{aligned} \quad [26]$$

where

$$\begin{aligned} x(t) &= \begin{bmatrix} q(t) \\ \omega(t) \\ S(t) \end{bmatrix}, \quad \tilde{x}_0 = \begin{bmatrix} e_0 \\ \omega(0) \\ s_0 \end{bmatrix}, \quad \theta = \begin{bmatrix} M_P \\ B_s V \\ H_c \\ \nu \end{bmatrix} \\ \nu &= H_c k \\ J(x(t), t) &= \|q(t) \otimes c_{ECI}(t) \otimes q(t)^{-1} - c_{bus}(t)\| \\ g(\tilde{x}_0) &= \begin{bmatrix} q(e_0) \\ \omega(0) \\ k(s_0 H_c + H(0)) \end{bmatrix} \\ f(x(t), \theta, t) &= \begin{bmatrix} \frac{1}{2} \omega(t) \otimes q(t) \\ I^{-1} \left( \left( \frac{2}{\pi} B_s V \arctan(S(t)) + \dots \right) \right. \\ \left. \mu_0 M_P \times H(t) \right) - \omega(t) \times I \omega(t) \\ \left. k \dot{H}(t) \left( \frac{H(t) - \frac{S(t)}{k} \pm H_c}{2 H_c} \right)^2 \right) \end{bmatrix} \\ H(t) &= q(t) \otimes H_{ECI}(t) \otimes q^{-1}(t) \\ \dot{H}(t) &= q(t) \otimes \dot{H}_{ECI}(t) \otimes q^{-1}(t) - H(t) \end{aligned} \quad [27]$$

A fixed time step RK4 algorithm is used to perform the integration. For numerical stability, the time step  $dt$  is chosen to ensure that  $\|\omega dt\| \ll 1$ .

## II.IX Initialization

The problem as detailed in Equations [26] and [27] is highly non-convex and the cost function is chaotic in the initial conditions. Regardless of the numerical optimization method used to solve the problem, a good initial guess

will be critical to finding the minimum, corresponding to the best fit.

Initial estimates for the magnetic properties are best taken from laboratory tests. As has been shown in previous papers,<sup>3,6</sup> material data sheets cannot be relied upon for accurate hysteresis parameters. If no pre-launch test data is available for the samples installed then estimates should be made based upon tests of similar materials.

A good estimate for the initial angular rate  $\omega(0)$  can be found by examining the frequency content of the bus data. A sample power spectral density for the RAX-1 spacecraft solar vector data is shown in Figure 4. In steady state it can be assumed that the spacecraft will be spinning around the permanent dipole, so an initial angular rate aligned with the permanent dipole and with the same magnitude as the peak in the power spectral density will be a reasonable initial guess. There still exists an ambiguity as to the direction of rotation about the permanent dipole, so the optimization may need to be run starting in both cases.

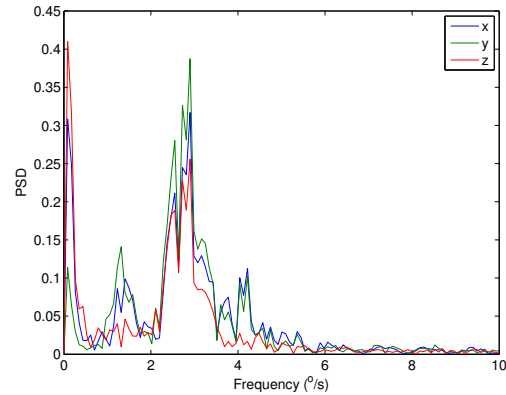


Figure 4: Power Spectral Density obtained from performing FFT of the solar vector bus data from RAX-1

An initial attitude direction cosine  $R$  matrix can be estimated by solving Wahba's problem<sup>7</sup> at  $t = 0$ . Wahba's problem determines the rotation matrix between two frames that best satisfies observations of vectors in both frames. A minimum of two independent vectors measured or known in both the body frame and inertial frame are required to produce a solution. The two vectors are the sun unit vector  $c$  and the local external magnetic field  $H$ , both of which are known in the inertial frame. The sun vector is known even in a severely sensor deprived case via solar panel current measurements. If a magnetometer is available, this can be used to estimate the magnetic field vector in the body frame. If no magnetometer data is available, a weaker assumption can be made that the permanent dipole is aligned to the magnetic field. This will likely

be a reasonable estimate once the spacecraft is operating at steady state. Following the method of Markeley<sup>8</sup> that uses singular value decomposition to solve Wahba's problem, an initial estimate of the attitude matrix  $R$  is found using Equation [28]. Converting from an attitude matrix to Euler Angles is trivial.

$$\begin{aligned} B &= H_{body} H_{ECI}^T + c_{body} c_{ECI}^T \\ B &= U \Sigma V^T \\ R &= U \text{diag} \left( \begin{bmatrix} 1 & 1 & \det(U) \det(V) \end{bmatrix} \right) V^T \quad [28] \end{aligned}$$

### III. RESULTS

The optimization algorithm was run on data from the O/OREOS and RAX-1 spacecraft. In both cases the cost function only included solar vector measurements. RAX-1 included magnetometer data which allowed for a better estimate of the initial kinematic state. The MATLAB 'active-set' algorithm was used.

#### III.I Data Sources

Nano satellites seldom have extensive sensor suites. However one vector that is almost always observable is the sun vector. Spacecraft typically monitor currents from solar panels, so even if the spacecraft carries no photodiodes an estimate of the sun vector can still be made by filtering and calibrating the panel currents.

The Organism/Organic Exposure to Orbital Stresses (O/OREOS) spacecraft is a 3U nano satellite that launched in November 2010 from Kodiak, AK into an approximately 650 km altitude, 72° low Earth orbit. O/OREOS carried two astrobiology payloads to study the survivability and viability of the space environment to live organisms and organics respectively. The O/OREOS spacecraft passive attitude stabilization system consisted of permanent dipoles along the long axis, and hysteresis rods in the plane perpendicular to the long axis. O/OREOS had no direct onboard attitude sensing, however the spacecraft bus did monitor solar panel currents. After calibrating and filtering the panel currents a rudimentary estimate of the  $x$  and  $y$  components of the solar vector can be obtained.

Included on the same launch manifest as O/OREOS was the first Radio Aurora Explorer satellite, RAX-1 a 3U CubeSat illustrated in Figure 5 that was developed to study magnetic field-aligned plasma irregularities in Earth's ionosphere.<sup>9</sup> The satellite was developed jointly by SRI International and the University of Michigan and the science payload is an ultra high frequency (UHF) radar receiver. Working in conjunction with ground based incoherent scatter radar stations, the purpose of the mission was to improve the understanding of the ionospheric irregularities with the ultimate goal of enabling short-term forecasting. The passive magnetic attitude control system consists of four permanent magnets aligned with the

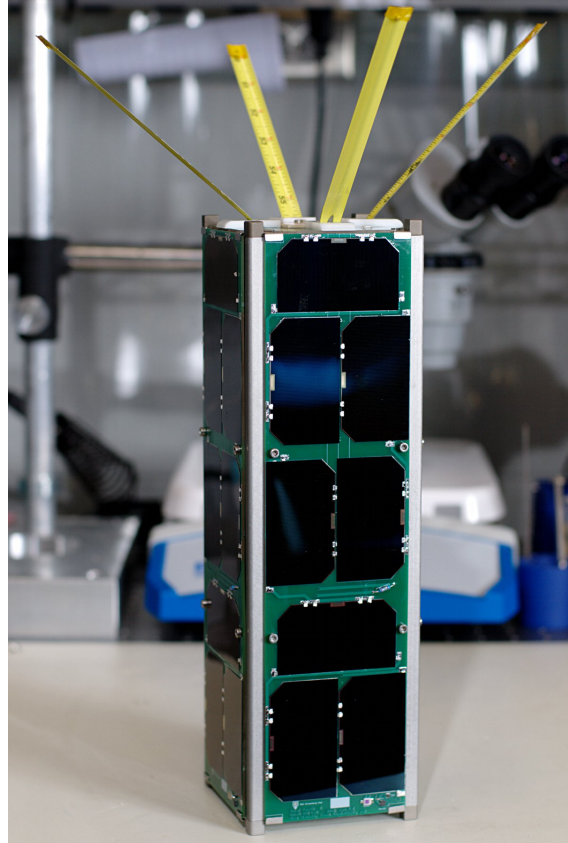


Figure 5: University of Michigan RAX-1 3U Cubesat

long  $z$  axis and two strips of HyMu80 soft magnetic material mounted in two axes perpendicular to the permanent magnets. RAX-1 included a full suite of attitude sensors comprising of multiple photodiodes, two three-axis magnetometers, and a three-axis rate gyroscope.<sup>10</sup> To improve the accuracy of the magnetometer and photodiode measurements attitude independent calibration was performed, with an on-orbit magnetometer calibration algorithm developed to mitigate the effect of nearby electronics on the magnetometers, which are embedded in the spacecraft.<sup>11</sup> The calibrated photodiode readings were used to create a reliable estimate of the sun vector in the body frame. In the work described in this paper the calibrated magnetometer data was used for initialization of the optimization algorithm and verification of the solution. The gyro data was used solely for verification of the solution.

Both O/OREOS and RAX-1 recorded data at 1Hz. TLE ephemerides were available for both spacecraft with updates occurring about every twenty four hours, leading to maximum orbit propagation errors of a few kilometers.

### III.II Steady State – O/OREOS

When solving for steady state, the magnetically permeable materials were assumed to not be present by enforcing  $B_s V = 0$ , so only the initial kinematic state and the permanent dipole are solved for. Ignoring the permeable material is a reasonable assumption based on the physics and purpose of damping. Additionally the permanent dipole only case provides a simpler problem for the optimization algorithm to solve.

Figure 6 shows a plot of the solar vector as measured by O/OREOS and the solar vector as computed by the simulation with initial conditions and parameters as solved by the optimization algorithm. As can be seen in Fig-

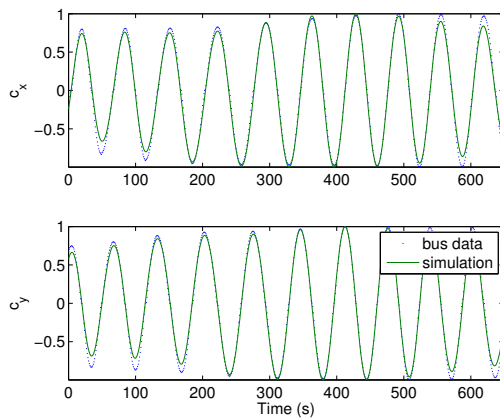


Figure 6: Comparison of solar vector components for O/OREOS. 11-Apr-2011 20:23:41 UTC

ure 6 the simulated solar vector matches well with the estimated solar vector obtained from solar panel currents. Using laboratory measurements of similar hardware, the total  $z$ -aligned dipole for O/OREOS was estimated to be  $15.5 \text{ Am}^2$ . The optimized value for the permanent dipole was  $[0.31, -0.02, 16.9]^T \text{ Am}^2$ , which is not dissimilar from the assumed installed value.

The solved permanent dipole is close to  $z$ -aligned and has a reasonable order of magnitude. To demonstrate the problems with using the incorrect dipole, the optimization was run again on the same data set, but forcing the modeled permanent dipole strength  $M_P$  to the pre-launch measured value. The best cost function obtained was over four times larger than that found by calibrating the dipole. The solar vector generated from simulation is shown in Figure 7, where the phase can be seen to be slipping obviously within ten minutes of the start of the data set.

An attempt to verify the solved permanent dipole can be made by performing the optimization on a different data set. Figure 8 shows the result of a second optimization run on a different data set. In this second case the optimal permanent dipole was found to be  $[0.35, 0.02, 19.8]^T \text{ Am}^2$ ,

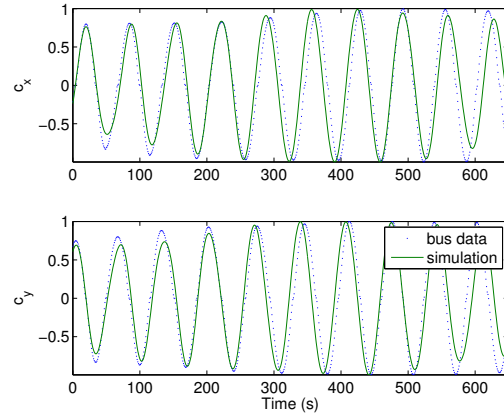


Figure 7: Comparison of solar vector components for O/OREOS. 11-Apr-2011 20:23:41 UTC. Pre-launch dipole assumed. Note developing phase error in estimation.

which is similar but not the same. It is possible that the parameters were over-fitted to the data which is made more likely due to the short available data run and having only  $x$  and  $y$  components available.

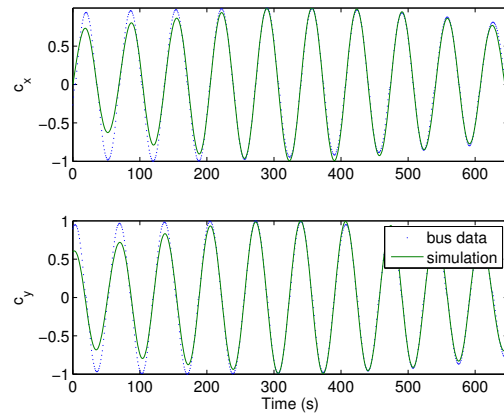


Figure 8: Comparison of solar vector components for O/OREOS. 04-Apr-2011 21:00:02 UTC

To test for over-fitting, a final optimization was performed that found two sets of initial conditions and a single permanent dipole that best explained both sets of data. This jointly optimized permanent dipole was found to be  $[0.30, 0.00, 17.4]^T \text{ Am}^2$ . The cost functions associated with each optimization are given in Table 2. The jointly optimized dipole is still a close fit, with little cost difference to the individually optimized dipoles.

Dipole Optimization Used	04-Apr-2011 21:00:02 UTC	11-Apr-2011 20:23:41 UTC
None (pre-launch)	0.1178	0.3764
Individual	0.1036	0.0812
Joint	0.1047	0.0819

Table 2: Cost functions for optimization of the permanent dipole and initial attitude for two data sets for the O/OREOS spacecraft.

### III.III Steady State – RAX-1

While the results from the optimization on O/OREOS look promising, little hard conclusions can be drawn about the success of the algorithm due to the scarcity of the data and the limited sensor suite available. By contrast RAX-1 offered richer data sets both in terms of having longer time periods of data collection, and of having more sensors that can be used for verification.

The optimization was run for data from RAX-1, with a sample set of results shown in Figure 9. For clarity in the figure, only the first 1500 seconds of the data run are shown.

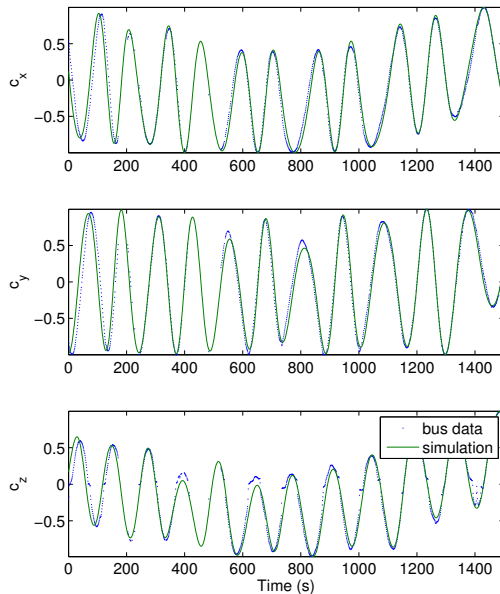


Figure 9: Comparison of solar vector components for RAX-1. 30-Dec-2010 14:28:15 UTC

Before launch the  $z$ -aligned permanent dipole was assumed to be  $3.2\text{Am}^2$ . The algorithm returned an optimal dipole of  $[0.25, 0.07, 1.06]^T\text{Am}^2$ , markedly different from the pre-launch value both in magnitude and alignment. Figure 10 illustrates the best fit over the same dataset if the pre-launch dipole was used in the dynam-

ics model, and shows how quickly the observed and simulated data diverge. The cost functions associated with each optimization are listed in Table 3.

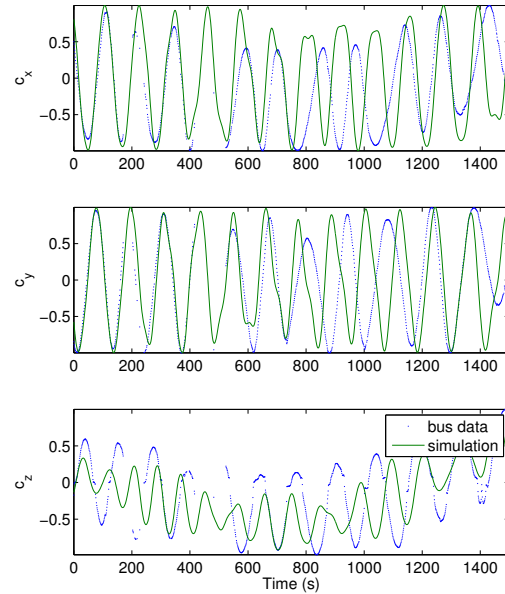


Figure 10: Comparison of solar vector components for RAX-1. 30-Dec-2010 14:28:15 UTC. Pre-launch assumed dipole used. Note large errors between observed data and simulation.

The RAX-1 spacecraft also includes magnetometer and gyros, and as the data from these sensors were not used in the cost function or constraints they can be used to verify the simulated attitude profile. Figure 11 compares the calibrated magnetometer readings to those generated by the simulation and Figure 12 compares the onboard gyro data to the angular rates from the simulation. The magnetometer readings agree closely. The gyro readings have more error, but that would be expected as the gyros have a bias.

As was done for the data from O/OREOS, an optimization was also performed on a different set of data from RAX-1. Figure 13 is a comparison of solar vector readings and simulated sun vectors for a data set taken fifteen days earlier. The optimized dipole from this data set is  $[0.25, 0.08, 1.04]^T\text{Am}^2$ , which is within 2% of the optimal dipole from the previous RAX-1 dataset studied. The closeness of the two optimal dipoles and the cross check against independent bus data build a strong case for the validity of the dynamics model and solved parameters.

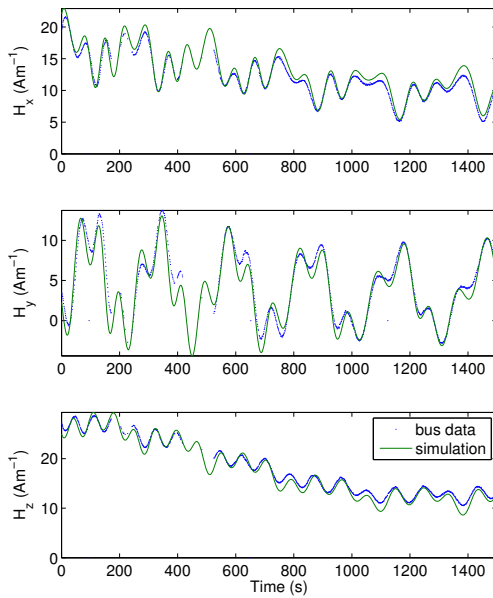


Figure 11: Comparison of magnetometer readings to magnetic field in the body frame as generated by the simulation. RAX-1. 30-Dec-2010 14:28:15 UTC

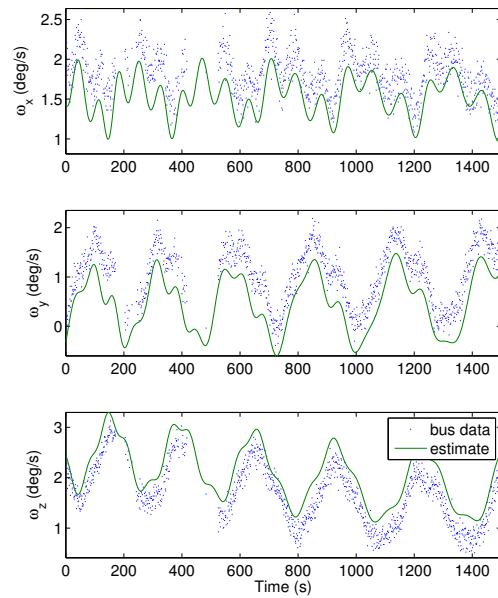


Figure 12: Comparison of IMU gyro readings to angular rates as generated by the simulation. RAX-1. 30-Dec-2010 14:28:15 UTC

Dipole Optimization Used	15-Dec-2010 17:36:09 UTC	30-Dec-2010 14:28:15 UTC
None (pre-launch)	0.9976	0.9090
Individual	0.1619	0.1636

Table 3: Cost functions for optimization of the permanent dipole and initial attitude for two data sets for the RAX-1 spacecraft.

### III.IV De-Tumbling Phase

Figure 14 shows the result of the optimization for an earlier dataset from RAX-1, again assuming only a permanent dipole and no permeable material. Two thousand seconds of data was included in evaluating the cost function. Only the middle thousand seconds are shown in Figure 14 for clarity. As can be seen from Figure 14 it appears that the attitude dynamics resulting from just the dipole are insufficient to explain the readings observed. This is especially true after the the 1000 second mark where the  $x$  and  $y$  components diverge. In order to get good data agreement permeable material needs to be included in the estimation. Figure 15 shows the result of a full optimization over the earlier dataset where permeable material was included. The match is improved but is still not as good as in the steady state case.

### III.V Computational Notes

When running the full parameter optimization, over five thousand function evaluations were required. Each function evaluation involves propagating the spacecraft for several thousand time steps. Without utilizing the numerical substitution described in Equation [11], a complete optimization would have taken hours to run, as opposed to only minutes with the substitution.

## IV. CONCLUSION

An optimization framework was developed that validates the assumed spacecraft dynamics model, calibrates the magnetic material properties and provides an estimate of the attitude of the spacecraft. The resultant parameters found through the optimization remain physically realizable. The importance of on orbit calibration of magnetic properties was shown as even in steady state when only a permanent dipole was assumed, the permanent dipole that best explained the observed data differed from pre-launch measurements. Initial studies of the de-tumbling shows that a single permanent dipole cannot adequately explain the data, but more work needs to be done to be able to accept the validity of the proposed hysteresis model.

## V. ACKNOWLEDGEMENTS

The research described in this paper was funded by a grant from NASA Ames Research Center. Orbital data

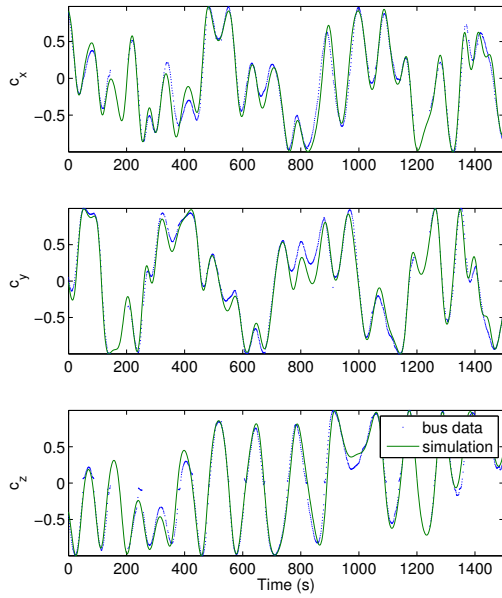


Figure 13: Comparison of solar vector components for RAX-1. 15-Dec-2010 17:36:09 UTC

for the O/OREOS spacecraft was provided by Santa Clara University. Orbital data for the RAX-1 spacecraft was provided by the University of Michigan. RAX-1 was funded by the U.S. National Science Foundation

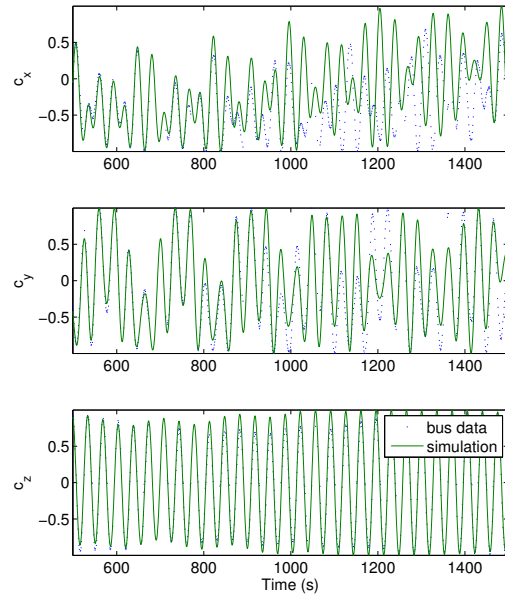


Figure 14: Comparison of solar vector components for RAX-1. Only permanent dipole modeled. 01-Dec-2010 08:30:46 UTC

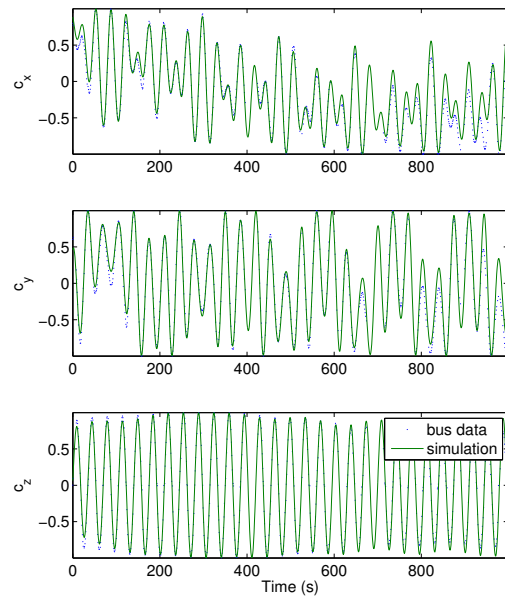


Figure 15: Comparison of solar vector components for RAX-1. Full magnetic system modeled. 01-Dec-2010 08:30:46 UTC

## VI. NOTATION

Symbol	Description	Units
$\mu_0$	permeability of free space $= 4\pi \times 10^{-7}$	$\text{Hm}^{-1}$
$H$	external magnetic field, body frame	$\text{Am}^{-1}$
$H_{ECI}$	Earth's magnetic field, ECI frame	$\text{Am}^{-1}$
$H_c$	coercivity of permeable material	$\text{Am}^{-1}$
$B$	induced magnetic flux den- sity in a permeable mate- rial	T
$B_r$	remanence flux density of permeable material	T
$B_s$	saturation flux density of permeable material	T
$V$	volume of permeable mate- rial	$\text{m}^3$
$M$	total dipole of magnetic material	$\text{Am}^2$
$M_P$	permanent dipole in a per- manent magnet	$\text{Am}^2$
$I$	moment of inertia, body frame	$\text{kgm}^2$
$T$	external torque, body frame	Nm
$\omega$	angular rate, body frame	$\text{rad s}^{-1}$
$q$	unit quaternion, inertial to body frame	

## REFERENCES

- [1] Flatley, T. W. and Henretty, D. A., "A Magnetic Hysteresis Model," *Flight Mechanics/Estimation Theory Symposium 1995*, edited by K. R. Hartman, May 1995, pp. 405–415.
- [2] Bleier, T., Clarke, P., Cutler, J., DeMartini, L., Dunson, C., Flagg, S., Lorenz, A., and Tapio, E., "Quakesat lessons learned: Notes from the development of a triple cubesat," 2004.
- [3] Burton, R., Starek, J., and Rock, S. M., "A New Method for Simulating the Attitude Dynamics of Passively Magnetically Stabilized Spacecraft," *Proceedings of the 22nd AAS/AIAA Space Flight Mechanics Meeting*, AAS/AIAA, AAS/AIAA, Charleston SC, 2012.
- [4] International Association of Geomagnetism and Aeronomy, Working Group V-MOD. Participating members, Finlay, C. C., Maus, S., Beggan, C. D., Bondar, T. N., Chambodut, A., Chernova, T. A., Chulliat, A., Golovkov, V. P., Hamilton, B., Hamoudi, M., Holme, R., Hulot, G., Kuang, W., Langlais, B., Lesur, V., Lowes, F. J., Lühr, H., Macmillan, S., Manda, M., McLean, S., Manoj, C., Menvielle, M., Michaelis, I., Olsen, N., Rauberg, J., Rother, M., Sabaka, T. J., Tangborn, A., Tøffner-Clausen, L., Thébaud, E., Thomson, A. W. P., Wardinski, I., Wei, Z., and Zvereva, T. I., "International Geomagnetic Reference Field: the eleventh generation," *Geophysical Journal International*, Vol. 183, No. 3, 2010, pp. 1216–1230.
- [5] Vallado, D., Crawford, P., Hujsak, R., and Kelso, T., "Revisiting spacetrack report# 3," *AIAA*, Vol. 6753, 2006, pp. 2006.
- [6] Santoni, F. and Zelli, M., "Passive magnetic attitude stabilization of the UNISAT-4 microsatellite," *Acta Astronautica*, Vol. 65, No. 5-6, 2009, pp. 792 – 803.
- [7] Wahba, G. et al., "A least squares estimate of satellite attitude," *Siam Review*, Vol. 7, No. 3, 1965, pp. 409.
- [8] Markley, F., "Attitude determination using vector observations and the singular value decomposition," *The Journal of the Astronautical Sciences*, Vol. 36, No. 3, 1988, pp. 245–258.
- [9] Cutler, J., Springmann, J., Spangelo, S., and Bahcivan, H., "Initial Flight Assessment of the Radio Aurora Explorer," *proceedings of the 25th Annual AIAA/USU Conference on Small Satellites. SSC11-VI-6. Logan, Utah*, 2011.
- [10] Springmann, J., Sloboda, A., Klesh, A., Bennett, M., and Cutler, J., "The attitude determination system of the RAX satellite," *Acta Astronautica*, Vol. 75, 2012, pp. 120–135.
- [11] Springmann, J., "Attitude-Independent Magnetometer Calibration with Time-Varying Bias," *Proceedings of the 25th Annual Small Satellite Conference*, 2011.